sEMG-Based Adaptive Cooperative Multi-Mode Control of a Soft Elbow Exoskeleton Using Neural Network Compensation

Qingcong Wu, *Member, IEEE*, Zhijie Wang, and Ying Chen

***Abstract*— Soft rehabilitation exoskeletons have gained much attention in recent years, striving to assist the paralyzed individuals restore motor functions. However, it is a challenge to promote human-robot interaction property and satisfy personalized training requirements. This article proposes a soft elbow rehabilitation exoskeleton for the multi-mode training of disabled patients. An adaptive cooperative admittance backstepping control strategy combined with surface electromyography (sEMG)-based joint torque estimation and neural network compensation is developed, which can induce the active participation of patients and guarantee the accomplishment and safety of training. The proposed control scheme can be transformed into four rehabilitation training modes to optimize the cooperative training performance. Experimental studies involving four healthy subjects and four paralyzed subjects are carried out. The average root mean square error and peak error in trajectory tracking test are 3.18° and 5.68°. The active cooperation level can be adjusted via admittance model, ranging from 4.51 °/Nm to 10.99 °/Nm. In cooperative training test, the average training mode value and effort score of healthy subjects (i.e., 1.58 and 1.50) are lower than those of paralyzed subjects (i.e., 2.42 and 3.38), while the average smoothness score and stability score of healthy subjects (i.e., 3.25 and 3.42) are higher than those of paralyzed subjects (i.e., 1.67 and 1.71). The experimental results verify the superiority of proposed control strategy in improving position control performance and satisfying the training requirements of the patients with different hemiplegia degrees and training objectives.**

Manuscript received 5 February 2023; revised 12 July 2023 and 3 August 2023; accepted 12 August 2023. Date of publication 17 August 2023; date of current version 25 August 2023. This work was supported in part by the National Natural Science Foundation of China under Grant 52175014, in part by the Natural Science Foundation of Jiangsu Province under Grant BK20211183, in part by the Fundamental Research Funds for the Central Universities under Grant NS2023024, and in part by the Postgraduate Research and Practice Innovation Program of Nanjing University of Aeronautics and Astronautics (NUAA) under Grant xcxjh20220505. *(Corresponding author: Qingcong Wu.)*

This work involved human subjects or animals in its research. Approval of all ethical and experimental procedures and protocols was granted by the Institutional Review Board of Nanjing University of Aeronautics and Astronautics under Application No. IRB [2022]-178.

Qingcong Wu and Zhijie Wang are with the College of Mechanical and Electrical Engineering, Nanjing University of Aeronautics and Astronautics, Nanjing, Jiangsu 210016, China (e-mail: wuqc@nuaa.edu.cn; wangzj_nuaa@126.com).

Ying Chen is with the College of Continuing Education, Nanjing University of Aeronautics and Astronautics, Nanjing, Jiangsu 210016, China (e-mail: chenying_nuaa@nuaa.edu.cn).

Digital Object Identifier 10.1109/TNSRE.2023.3306201

***Index Terms*— Soft elbow exoskeleton, adaptive cooperative multi-mode control, sEMG, neural network compensation, active participation.**

I. Introduction

THE statistics from the World Health Organization indicate that about 15 million people worldwide suffer from stroke every year [1]. More than 80% of the stroke survivors have to experience motor dysfunction, and they require a large number of rehabilitation training to regain motor abilities. In traditional clinical movement therapy, recovery training has been manually assisted by physiotherapists. However, there are several disadvantages in manual one-to one training, such as the large consumption of labor and time, the high cost of treatment, the limited hospital human resources, and the dependence on the ability of physiotherapist [2]. In recent years, the robotic devices for rehabilitation training has attracted the attention of researchers due to its advantages of sparse labor, high training intensity, good repeatability, and task orientation [3].

Exoskeleton has emerged as one of the effective solutions in robotic-assisted rehabilitation training [4]. It can be worn on the affected limb of patient to provide required motion assistance. Currently, the majority of existing rehabilitation exoskeletons have rigid mechanical structures [5], [6], [7]. They can work in parallel with human limbs, apply driving torques to human joints, support compressive forces, and transmit forces to ground [8], [9], [10]. However, rigid exoskeletons suffer from inherent heavy weight, bulky size, high power consumption, restricted freedom and misalignment between robot and human joints, leading to unsafety and discomfort for patients [11].

Due to the drawbacks with rigid structures, soft exoskeletons made from lightweight and soft materials become a promising alternative [12], [13], [14]. They used garment-like functional textiles and compliant actuators to interface with human body and improve interaction compatibility. Tan et al. [15] designed a cable-driven soft exoskeleton to reduce metabolic cost during human walking. Martin et al. [16] developed a myoelectric control strategy for a soft hand rehabilitation exoskeleton using kinematics synergies. Proietti et al. [17] presented a wearable soft shoulder-elbow rehabilitation exoskeleton driven by textile

pneumatic actuator. Hosseini et al. [18] designed a soft exosuit with twisted string actuators to execute elbow assistive tasks. Compared to rigid structures, soft exoskeletons can improve comfort, flexibility, coordination and safety for wearers.

The quality of robot-assisted rehabilitation therapy is directly affected by the applied controller. State-of-the-art rehabilitation exoskeleton control strategies can be divided into two types based on patient's participation degree: patient-passive control and patient-cooperative control. The patient-passive control is applicable for severely impaired hemiplegic subjects without any motor ability, preventing muscle atrophy and joint spasm deformation. In this case, exoskeleton is demanded to drive the affected limb to passively and repeatedly follow a predefined motion trajectory. Many trajectory-tracking control strategies for passive training have been developed, such as proportional-integral-derivative control (PID) [19], backstepping control [20], time-delay control [21], terminal sliding mode control [22], computed torque control [23], and so on.

Clinical rehabilitation research shows that the active participation is fundamental in inducing neural plasticity and optimizing neuromuscular recovery [24], [25]. Thus, for the hemiplegic subjects who have regained partial motor capacity, the patient-cooperative control should be applied to modulate robotic assistance based on the intention and need of patients, intervening minimally so as to promote involvement. Chen et al. [26] designed an adaptive impedance patient-cooperative controller for a lower limb exoskeleton. The interaction torques between are estimated via neural network. Hamed et al. [27] came up with an assist-as-needed controller defined in velocity domain to modulate the impedance of exoskeleton and provide appropriated support during robot-aided training. Pehlivan et al. [28] designed a minimal assist-as-needed control scheme for arm rehabilitation exoskeleton, using model-based sensorless force estimation to determine patient capability. Similarly, a minimal-intervention-based control strategy was presented in [29]. Aliasgar et al. [30] came up with a stability-guaranteed assistance regulation admittance controller to facilitate robot-assisted training task and encourage user effort.

Nevertheless, many of the current cooperative controllers are developed for rigid exoskeletons. Compared with the control of rigid exoskeletons, the researches on the robust cooperative control of soft exoskeletons are more challenging due to the inherent nonlinear compliance property of soft structures. The cooperative control of rigid exoskeleton can be designed based on the human-robot dynamics to improve control accuracy [27], [29], [30]. However, for soft exoskeleton, it is difficult to obtain the completed dynamics model involving biological force, soft tissue and flexible deformation [31]. Thus, the cooperative control of soft exoskeleton is generally not based on dynamics [18], [32], and the training mode is single and cannot meet the requirements of different patients. Chen et al. [33] developed a PID-based modeless optimization control strategy for a soft hip-assistive exosuit. Similarly, Ismail et al. [34] came up with a proportional-integral (PI) controller for a soft exoskeleton to assist elbow rehabilitation training. Siviy et al. [35] developed a low-level velocity controller without entire dynamics model for a soft exoskeleton to augment ankle power.

Based on the above discussion, a new adaptive admittance backstepping sliding mode control strategy is developed in our work for a soft elbow exoskeleton, assisting disabled patients conduct multi-mode cooperative rehabilitation training. The dynamic modeling errors and disturbances of robot system are compensated via a neural network observer. A position-error-based adaptive admittance model is proposed to adjust human-robot interaction features and encourage active participation. The control scheme can be switched to four training modes to meet the needs of patients in different training conditions, i.e., passive-training mode, active-training mode, assist-as-needed training mode, and safety mode. The stability of the closed-loop controller is analyzed via the Lyapunov theory. Verification experiments are conducted on four healthy subjects and four stroke patients, and the results were discussed and analyzed.

Compared with the previous works, the contributions of this paper are as follows:

1) A newly adaptive cooperative admittance backstepping sliding mode control scheme is proposed to realize multi-mode soft exoskeleton-assisted rehabilitation training, satisfying the training requirements of patients with different hemiplegia degrees. As far as we know, this has never been reported in the existing literature.
2) The human-soft exoskeleton coupling dynamic model is established. The human elbow joint torque is obtained based on the Kalman filter and the surface electromyography signals (sEMG) from biceps and triceps. The lumped effects of dynamics modeling errors and external disturbances are estimated through a Gaussian radial basis function network.

This paper is organized as follows. Section II introduces the development of soft exoskeleton and adaptive cooperative admittance backstepping control scheme. Section III describes the proposed experimental protocol. The results and discussion are given in Section IV. A conclusion is drawn in Section V.

II. Methodology

A. Soft Elbow Exoskeleton Description

Fig. 1 shows the structure and major components of the proposed wearable soft elbow exoskeleton system, which was designed to assist the disabled patient perform multi-mode rehabilitation training. The patient can be equipped with the exoskeleton via the wearable soft suit composing of base layer, adjustable soft wraps and auxiliary Velcro straps. The device utilized compliant tendon-sheath actuator mounted on the backside of wearer to deliver remote driving torque to the upper limb in the direction of elbow flexion and extension, as shown in Fig. 1(a) and Fig. 1(b). The compliant tendon-sheath actuator was developed based on the Hill-type muscle model and made up of flexible tendon sheath units, tension/compression springs and servo motors (SGM7G, YASKAWA Inc.) [36]. Several sheath supports, guidance mechanisms and anchor points were mounted on the upside,

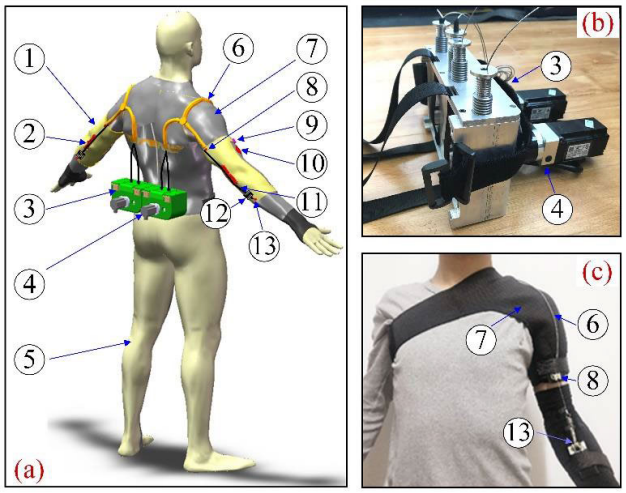

Fig. 1. Overview of the developed soft elbow exoskeleton. (a) CAD model of the soft elbow exoskeleton (1-Soft wrap; 2-Guidance mechanism; 3-Actuator unit; 4-Servo motor; 5-Wearer; 6-Outer sheath; 7-Base layer; 8-Sheath support; 9-Inertial measurement unit (IMU); 10-sEMG sensor; 11-Inner tendon; 12-Force sensor; 13-Anchor point); (b) The compliant tendon-sheath actuator; (c) The soft wearable exoskeleton suit worn on a subject.

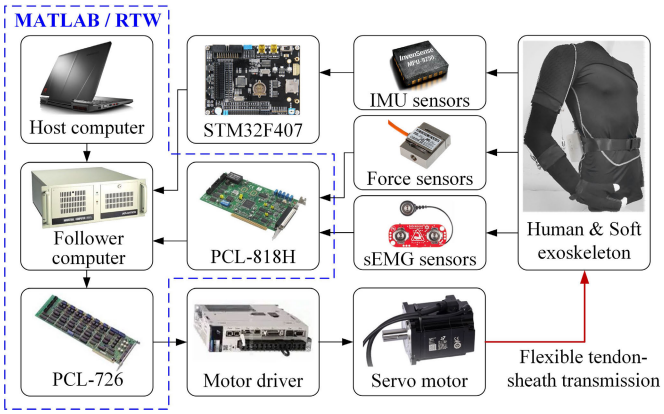

Fig. 2. The hardware architecture of real-time control system.

backside and underside of soft wrap respectively, in order to transmit the pulling force from outer sheathes and inner tendons to elbow joint. The transmission path of tendon-sheath units were optimized to pass through the center of rotation of shoulder. It contributes to eliminating the additional torque acting on undesirable joint and improving wear comfort. The flexibility property of the wearable soft suit allows it to mold to the body shape of the patient with a height ranging from 1.5 m to 2 m, as shown in Fig. 1(c). To guarantee training safety, the actuator was integrated with mechanical end stops to avoid excessive flexion and extension.

The soft exoskeleton was controlled via a MATLAB/RTW-based real-time control system (2016a, Mathworks Inc.) with a closed-loop dual-machine hierarchical architecture, as shown in Fig. 2. A laptop computer (ISK, Lenovo Inc.) with a graphical user interface was used to conduct the high-level host controller and generate Simulink-based control programs. Meanwhile, an industrial personal computer (610H, Advantech Inc.) was used as the low-level follower controller to execute

TABLE I
LIST OF ABBREVIATIONS

Abbreviation	Meaning
sEMG	surface Electromyography
IMU	Inertial Measurement Unit
PID	Proportional-Integral-Derivative
PI	Proportional-Integral
ABSMCNN	Admittance Backstepping Sliding Mode Control with Neural Network
SMC	Sliding Mode Control
ABSMC	Admittance Backstepping Sliding Mode Control
PTM	Passive Training Mode
ATM	Active Training Mode
AANTM	Assist-As-Needed Training Mode
STM	Safety Training Mode
RMSE	Root Mean Square Error
PE	Peak Error
ACL	Active Cooperation Level

embedded control commands and modulate the operation of exoskeleton [37]. The arm configuration detection was realized by four inertial measurement units (MPU9250, TELESKY Inc.) mounted at the upper arm and forearm of wearer. Besides, two miniature force sensors (JLBS-MD, KINGNO Inc.) were attached between the terminal of inner tendon and the anchor point to obtain the driving force acting on human elbow. The sEMG signals from the biceps and triceps of wearer were measured via a portable sEMG sensing system (Myoware, SparkFun Inc.) [38]. A 32-bit microcontroller (STM32F407, Microchip Inc.) was adopted to read the feedback signals from inertial measurement units and transmit them to follower controller through RS-232 serial port. The analog force signals and sEMG signals were acquired via two analog-to-digital converters (PCL-818H, Advantech Inc.) in follower computer. A digital-to-analog converter (PCL-726, Advantech Inc.) was used to convert the control instructions into corresponding analog voltage signals and communicate with motor drivers. The sampling frequency of the control loop was set to 1000 Hz.

B. Control Strategy Development

In this section, a new adaptive cooperative admittance backstepping sliding mode control strategy combined with neural network compensation (ABSMCNN) is developed for the above soft exoskeleton. It can assist the disabled patients with different degrees of hemiplegia carry out multi-mode rehabilitation training, including the passive-training mode training, the active-training mode training, the assist-as-needed training mode training, and the safety mode training. The overall block diagram of the proposed control scheme is elaborated in Fig. 3. All abbreviations used in this paper, including the abbreviations above, are given in Table I.

According to the dynamics analysis method of Lagrangian [39], the overall dynamic equation of the human-exoskeleton coupling system can be expressed in joint space as follow:

$$\tau(t) + \tau_h(t) = M\ddot{\theta}(t) + V\dot{\theta}(t) + G(t) + \tau_f(t) + D_u(t) \quad (1)$$

where $\tau(t)$ denotes the driving torque generated by the servo motor; $\tau_h(t)$ represents the elbow joint torque of wearer;

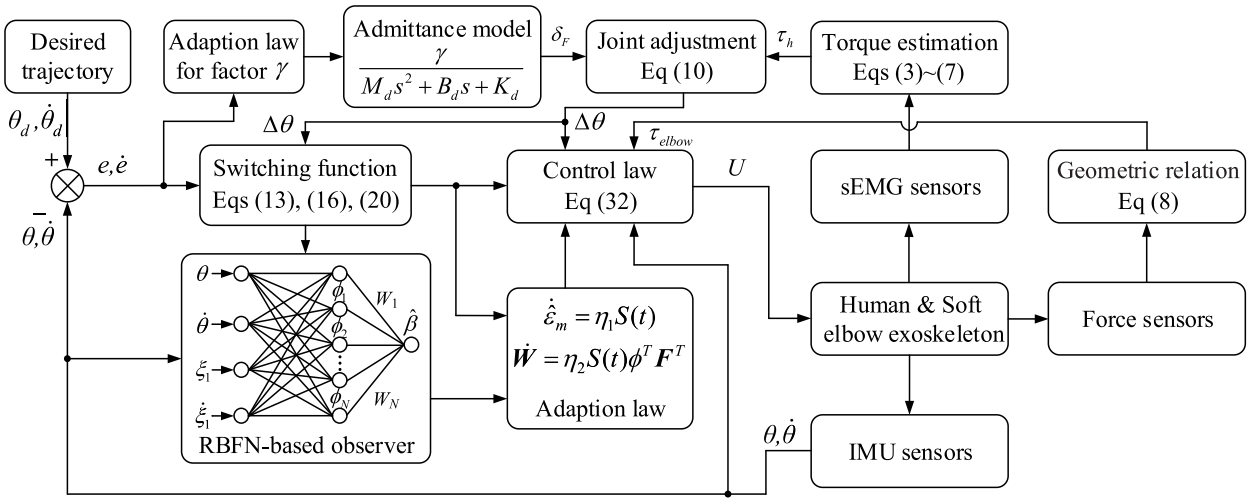

Fig. 3. Overall block diagram of the proposed neural network-based adaptive cooperative admittance backstepping control strategy.

$\theta(t)$, $\dot{\theta}(t)$ and $\ddot{\theta}(t)$ denote joint position, velocity and acceleration of elbow, respectively; M and V are the inertia and viscous damping coefficient of human-exoskeleton system; the gravitational torque is denoted as $G(t)$; the frictional torque is represented as $\tau_f(t)$, which mainly comes from the motor reducer and the tendon-sheath transmission component [40]; $D_u(t)$ represents the lumped effects of dynamics modeling errors and external disturbances.

From (1), since the inertia coefficient is positive, the acceleration of elbow can be given as follow:

$$\ddot{\theta}(t) = M^{-1}\left[\tau(t) + \tau_h(t) - V\dot{\theta}(t) - G(t) - \tau_f(t) - D_u(t)\right] \tag{2}$$

The elbow joint torque of human can be estimated in real time based on the sEMG signals from biceps and triceps [41]. Firstly, the raw sEMG signals were collected with a sampling frequency of 1 kHz. Next, a Butterworth filter with a passband of 10-500 Hz and a 50 Hz notch filter were adopted to remove undesirable noise. After that, a full wave rectifier and a 1 Hz low-pass Butterworth filter were utilized to generate the envelopes of sEMG signals. Then, the nonlinearly normalized sEMG signals EMG_N can be computed via the linearly normalized envelopes EMG_L as follow:

$$EMG_N = 100\frac{e^{(-EMG_L\rho)} - 1}{e^{(-100\rho-1)}} \tag{3}$$

Here, ρ is a constant defining exponential curvature.

Then, the human elbow joint torque can be estimated based on the Kalman filter. The state functions were defined as:

$$\tau_h(t) = \tau_h(t-1) + \delta \tag{4}$$

$$EMG_N(t) = \tau_h(t) + \varsigma \tag{5}$$

where $\tau_h(t\text{-}1)$ denotes the elbow joint torque at time before t; the covariance of process noise and measurement noise are represented as δ and ς. The prediction and update algorithms

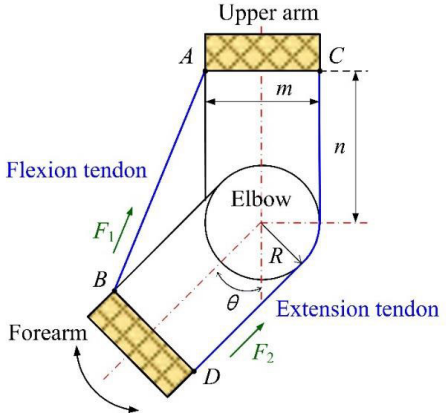

Fig. 4. Geometric diagram of the tendons routing on human elbow and soft wearable suit.

of the Kalman filter are defined as [42]:

$$\hat{\tau}_h(t|t-1) = \hat{\tau}_h(t-1|t-1) \tag{6}$$

$$\hat{\tau}_h(t|t) = \hat{\tau}_h(t|t-1) + \frac{E(t|t-1)}{E(t|t-1)+\varsigma}\left[EMG_N(t) - \hat{\tau}_h(t|t-1)\right] \tag{7}$$

where $\hat{\tau}_h(t-1|t-1)$, $\hat{\tau}_h(t|t-1)$ and $\hat{\tau}_h(t|t)$ are the previous, priori and posterior values of estimated joint torque; $E(t|t-1)$ is the priori error covariance. The estimated joint torque can be mapped into the actual joint torque via calibration tests.

The geometric diagram describing the relationships between the tendons routing on human elbow and soft wearable suit is depicted in Fig. 4. The flexion tendon and extension tendon are located on the front side and back side of elbow joint in agonist-antagonist configuration. They are pulled in different directions simultaneously to generate elbow driving torque. The pulling forces of flexion tendon and extension tendon are denoted as F_1 and F_2, respectively. The locations of the sheath supports mounted on the upside of soft wrap are denoted as point A and point C. Meanwhile, the locations of the anchor points mounted on the underside of soft wrap are

represented as point $C$and point D. The radius of wearer's elbow is represented as R. The width of the upper arm and forearm is assumed to be the same and denoted as m. The distance between the soft wrap and the elbow joint center is represented as n.

According to the geometric relationships shown in Fig. 3, the interaction torque acting on the elbow joint of wearer (i.e.,τ_{elbow}) can be calculated as follow:

$$\tau_{elbow}(t) = F_1(t)\sin\left[\frac{\theta(t)}{2} + \arctan(\frac{m}{2n})\right] \sqrt{n^2 + \frac{m^2}{4}} - F_2(t)R \tag{8}$$

Then, the frictional torque from motor reducer and tendon-sheath transmission can be obtained via the motor driving torque and the interaction torque as follow:

$$\tau_f(t) = K_r\tau(t) - \tau_{elbow}(t) \tag{9}$$

where K_r denotes the reduction ratio of motor reducer.

In order to adjust the human-robot interaction characteristics in different training modes and encourage patient's active participation, the desired admittance property between the soft elbow exoskeleton and human elbow can be given as follow:

$$\Delta\theta(t) = \tau_h(t)\cdot\delta_F \tag{10}$$

where

$$\delta_F = \frac{1}{M_d s^2 + B_d s + K_d}\gamma \tag{11}$$

Here,$\Delta\theta(t)$ is the desired joint angle adjustment value corresponding to the elbow joint torque generated by wearer; δ_F denotes the admittance model; the inertial gain, damping gain, and stiffness gain of admittance model are defined as M_d, B_d, and K_d, respectively. γ is an adaptive factor defined to modulate the interaction compliance during rehabilitation training.

The actual joint angle error of soft elbow exoskeleton can be obtained as follow:

$$e(t) = \theta_d(t) - \theta(t) \tag{12}$$

where$\theta_d(t)$ denotes the predefined desired trajectory of elbow joint;$e(t)$is the actual joint angle error.

The value of adaptive factor is determined according to the selected training mode and the absolute value of joint angle error, i.e., $|e|$. It can be divided into the following four cases:

1) Passive training mode (PTM). The adaptive factor is set to γ =0. The control purpose of this training mode is to assist the disabled patient passively follow a predefined training trajectory with high tracking accuracy, and the active motion intention of patient is ignored.
2) Active training mode (ATM). The joint angle error is within the range of $|e| \le R_a$, and the adaptive factor is set to $\gamma = \gamma_{\max}$. R_a is the boundary of active training region. $\gamma_{\max}$ is the predefined maximum adaptive factor which can achieve maximum interaction compliance. The control purpose of this training mode is to allow the patient to actively dominate the cooperative training trajectory by adjusting interaction torque τ_{elbow}.
3) Assist-as-needed training mode (AANTM). The joint angle error is within the range of $R_a < |e| \le R_n$, the adaptive factor is set to $\gamma = \gamma_{\max}[|e|(P\text{-}1)+R_a\text{-}PR_n]\cdot[P(R_a\text{-}R_n)]^{-1}$. Here, R_n is the boundary of assist-as-needed training region. P is a positive constant that determines the variation rate of interaction compliance. In this training mode, the rehabilitation robot judges that the patient has difficulty in actively and independently following the desired training trajectory. Thus, the interaction compliance level decreases linearly with the increase of actual joint angle error, ensuring that the affected limb can complete the training task with enough robot assistance.
4) Safety training mode (STM). In this case, the actual joint angle error satisfies the condition that $R_n < |e|$, and the adaptive factor is set to $\gamma = \gamma_{\max}\cdot\exp[(R_n\text{-}|e|)L^{-1}]\cdot P^{-1}$. In this training mode, the robot judges that the patient has come into an abnormal training state. The interaction torque increases exponentially with the increase of actual joint angle error, pulling the affected limb back to the desired training trajectory and avoiding collapse problem. Here, L is a predefined positive constant used to adjust the increase rate of interaction torque.

Furthermore, from (10) and (12), the admittance error$\xi_1(t)$ can be described as follow:

$$\xi_1(t) = e(t) - \Delta\theta(t) = \theta_d(t) - \theta(t) - \Delta\theta(t) \tag{13}$$

From (13), the time derivative of admittance error $\dot{\xi}_1(t)$ is given by

$$\dot{\xi}_1(t) = \dot{\theta}_d(t) - \dot{\theta}(t) - \Delta\dot{\theta}(t) \tag{14}$$

Then, the stabilizing function is defined and expressed as:

$$\alpha_1(t) = C\xi_1(t) \tag{15}$$

where $\alpha_1(t)$ is the stable coefficient; C is a positive constant.

The virtual control term can be given as:

$$\xi_2(t) = \dot{\xi}_1(t) + \alpha_1(t) = \dot{\theta}_d(t) - \dot{\theta}(t) - \Delta\dot{\theta}(t) + \alpha_1(t) \tag{16}$$

From (16), the time derivative of virtual control term $\dot{\xi}_2(t)$ is

$$\begin{aligned}\dot{\xi}_2(t) &= \ddot{\theta}_d(t) - \ddot{\theta}(t) - \Delta\ddot{\theta}(t) + \dot{\alpha}_1(t)\\ &= \ddot{\theta}_d(t) - \Delta\ddot{\theta}(t) + \dot{\alpha}_1(t)\\ &\quad - M^{-1}\left[\tau(t) + \tau_h(t) - V\dot{\theta}(t) - G(t) - \tau_f(t) - D_u(t)\right]\end{aligned} \tag{17}$$

Consider the first positive-definite Lyapunov function candidate as follow:

$$V_1 = \frac{1}{2}\xi_1^2(t) \tag{18}$$

Then, according to (14) and (16), the time derivative of V_1 can be expressed as

$$\begin{aligned}\dot{V}_1 &= \xi_1(t)\dot{\xi}_1(t)\\ &= \xi_1(t)\left[\dot{\theta}_d(t) - \dot{\theta}(t) - \Delta\dot{\theta}(t)\right]\\ &= \xi_1(t)\left[\xi_2(t) - \alpha_1(t)\right]\\ &= \xi_1(t)\xi_2(t) - C\xi_1^2(t)\end{aligned} \tag{19}$$

The switching function of sliding mode control can be designed as follow:

$$S(t) = \lambda\xi_1(t) + \xi_2(t) \tag{20}$$

where $S(t)$ denotes the sliding valuable; λ represents a positive proportional gain.

Differentiating $S(t)$ with respect to time and combining (17), we can obtain

$$\begin{aligned}\dot{S}(t) &= \lambda\dot{\xi}_1(t) + \dot{\xi}_2(t)\\ &= \lambda\dot{\xi}_1(t) + \ddot{\theta}_d(t) - \Delta\ddot{\theta}(t) + \dot{\alpha}_1(t)\\ &\quad - M^{-1}\left[\tau(t) + \tau_h(t) - V\dot{\theta}(t) - G(t) - \tau_f(t) - D_u(t)\right]\\ &= (\lambda + C)\dot{\xi}_1(t) + \ddot{\theta}_d(t) - \Delta\ddot{\theta}(t)\\ &\quad - M^{-1}\left[\tau(t) + \tau_h(t) - V\dot{\theta}(t) - G(t) - \tau_f(t) - D_u(t)\right]\end{aligned} \tag{21}$$

The preliminary control law U is designed as follow:

$$\begin{aligned}U = M\left[(\lambda + C)\dot{\xi}_1(t) + \xi_1(t) + \ddot{\theta}_d(t) + Ksign(S) - \Delta\ddot{\theta}(t)\right]\\ - \tau_h(t) + V\dot{\theta}(t) + G(t) + \tau_f(t)\end{aligned} \tag{22}$$

where K is a positive constant; sign $(\cdot)$ is a sign function.

$$sign(S) = \begin{cases} 1 \ if \ S(t) > 0 \\ 0 \ if \ S(t) = 0 \\ -1 \ if \ S(t) < 0 \end{cases} \tag{23}$$

Then, consider the second positive-definite Lyapunov function candidate as follow:

$$V_2 = V_1 + \frac{1}{2}S^2(t) \tag{24}$$

From (19), (21), (22), the time derivative of V_2 can be given:

$$\begin{aligned}&\dot{V}_2\\ &= \dot{V}_1 + S(t)\dot{S}(t)\\ &= \xi_1(t)\xi_2(t) - C\xi_1^2(t) + S(t)\dot{S}(t)\\ &= \xi_1(t)\xi_2(t) - C\xi_1^2(t)\\ &+ S(t)\begin{Bmatrix}(\lambda + C)\dot{\xi}_1(t) + \ddot{\theta}_d(t) - \Delta\ddot{\theta}(t)\\ -M^{-1}\left[\tau(t) + \tau_h(t) - V\dot{\theta}(t) - G(t) - \tau_f(t) - D_u(t)\right]\end{Bmatrix}\\ &= \xi_1(t)\left[\xi_2(t) - S(t)\right] - C\xi_1^2(t) - S(t)\left[Ksign(S) - M^{-1}D_u(t)\right]\\ &= -(\lambda + C)\xi_1^2(t) - S(t)\left[Ksign(S) - M^{-1}D_u(t)\right]\end{aligned} \tag{25}$$

Next, to estimate the lumped effects of dynamics modeling errors and external disturbances, a neural network observer is proposed based on a three-layer Gaussian radial basis function network. For simplification, we define

$$\beta = M^{-1}D_u(t) \tag{26}$$

The input vector of neural network $\boldsymbol{\Gamma}$ is selected as

$$\boldsymbol{\Gamma} = \left[\theta(t)\ \dot{\theta}(t)\ \xi_1(t)\ \dot{\xi}_1(t)\right] \tag{27}$$

The weighted sum method is utilized to obtain the output of neural network as follows:

$$\hat{\beta}(\boldsymbol{W}) = \boldsymbol{W}\boldsymbol{\phi} = \sum_{i=1}^{N} W_i\phi_i i = 1, 2, \cdots, N \tag{28}$$

$$\phi_i = \exp\left[-\frac{(\boldsymbol{\Gamma} - \boldsymbol{m}_i)^T(\boldsymbol{\Gamma} - \boldsymbol{m}_i)}{2b_i^2}\right] \tag{29}$$

where $\hat{\beta}(\boldsymbol{W})$ is the neural network output; N is the number of hidden nodes; W_i is the connective weight of the ith hidden layer and output layer; ϕ_i is the ith Gaussian function; $\boldsymbol{m}_i$ is the center vector of the ith neurons; b_i is the ith standard deviation.

Define the minimum approximation error ε_m as follow:

$$\varepsilon_m = \beta - \hat{\beta}(\boldsymbol{W}^*) \tag{30}$$

where $\boldsymbol{W}^*$ denotes an optimal connective weight vector achieving minimum approximation error.

Next, a neural network-based disturbance compensation control term is designed as follow:

$$U_{dis} = M\left[\hat{\varepsilon}_m + \hat{\beta}(\boldsymbol{W})\right] \tag{31}$$

where $\hat{\varepsilon}_m$ denotes the estimated value of ε_m.

Then, the final ABSMCNN control law can be obtained by combining (22) and (31), and we can get

$$\begin{aligned}U = M\left[(\lambda + C)\dot{\xi}_1(t) + \xi_1(t) + \ddot{\theta}_d(t) + Ksign(S) - \Delta\ddot{\theta}(t)\right]\\ - \tau_h(t) + V\dot{\theta}(t) + G(t) + \tau_f(t) + M\left[\hat{\varepsilon}_m + \hat{\beta}(\boldsymbol{W})\right]\end{aligned} \tag{32}$$

Consider the third positive-definite Lyapunov function candidate as follow:

$$V_3 = V_2 + \frac{1}{2\eta_1}(\varepsilon_m - \hat{\varepsilon}_m)^2 + \frac{1}{2\eta_2}(\boldsymbol{W}^* - \boldsymbol{W})\boldsymbol{F}^{-1}(\boldsymbol{W}^* - \boldsymbol{W})^T \tag{33}$$

Here, η_1 and η_2 represent two positive constants; $\boldsymbol{F}$ denotes a positive definite diagonal matrix.

According to (25), (32) and (33), the time derivative of V_3 can be given by

$$\begin{aligned}\dot{V}_3 &= \dot{V}_2 - \frac{1}{\eta_1}(\varepsilon_m - \hat{\varepsilon}_m)\dot{\hat{\varepsilon}}_m - \frac{1}{\eta_2}(\boldsymbol{W}^* - \boldsymbol{W})\boldsymbol{F}^{-1}\dot{\boldsymbol{W}}^T\\ &= -(\lambda + C)\xi_1^2(t)\\ &\quad - S(t)\left[Ksign(S) - M^{-1}D_u(t) + \hat{\varepsilon}_m + \hat{\beta}(\boldsymbol{W})\right]\\ &\quad - \frac{1}{\eta_1}(\varepsilon_m - \hat{\varepsilon}_m)\dot{\hat{\varepsilon}}_m - \frac{1}{\eta_2}(\boldsymbol{W}^* - \boldsymbol{W})\boldsymbol{F}^{-1}\dot{\boldsymbol{W}}^T\\ &= -(\lambda + C)\xi_1^2(t)\\ &\quad - S(t)Ksign(S) + S(t)\left[M^{-1}D_u(t) - \hat{\varepsilon}_m - \hat{\beta}(\boldsymbol{W})\right]\\ &\quad - \frac{1}{\eta_1}(\varepsilon_m - \hat{\varepsilon}_m)\dot{\hat{\varepsilon}}_m - \frac{1}{\eta_2}(\boldsymbol{W}^* - \boldsymbol{W})\boldsymbol{F}^{-1}\dot{\boldsymbol{W}}^T\\ &= -(\lambda + C)\xi_1^2(t) - S(t)Ksign(S)\\ &\quad + S(t)\left[\beta - \hat{\beta}(\boldsymbol{W}^*) - \hat{\varepsilon}_m\right]\\ &\quad + S(t)\left[\hat{\beta}(\boldsymbol{W}^*) - \hat{\beta}(\boldsymbol{W})\right] - \frac{1}{\eta_1}(\varepsilon_m - \hat{\varepsilon}_m)\dot{\hat{\varepsilon}}_m\\ &\quad - \frac{1}{\eta_2}(\boldsymbol{W}^* - \boldsymbol{W})\boldsymbol{F}^{-1}\dot{\boldsymbol{W}}^T\end{aligned} \tag{34}$$

TABLE II
CHARACTERISTICS OF THE SUBJECT CONDUCTING EXPERIMENTS

Sub	Gender	Age (years)	Height (m)	Weight (kg)	FMA score (upper limb)	Paralysis level
S1	male	29	1.81	76.7	66 (full)	healthy
S2	male	22	1.68	62.3	66 (full)	healthy
S3	female	37	1.60	51.2	66 (full)	healthy
S4	female	70	1.72	69.5	66 (full)	healthy
S5	male	53	1.77	70.6	63	slight
S6	female	61	1.58	45.3	61	slight
S7	male	58	1.71	55.9	49	moderate
S8	female	65	1.59	48.0	21	severe

Then, design the adaption laws for $\dot{\hat{\varepsilon}}_m$ and $\dot{\boldsymbol{W}}$ as follows:

$$\dot{\hat{\varepsilon}}_m = \eta_1 S(t) \tag{35}$$

$$\dot{\boldsymbol{W}} = \eta_2 S(t)\boldsymbol{\phi}^T \boldsymbol{F}^T \tag{36}$$

By combining (28), (30), (35) and (36) into (34), the time derivative of V_3 can be rewritten as

$$\begin{aligned}\dot{V}_3 &= -(\lambda + C)\xi_1^2(t) - S(t)Ksign(S) + S(t)(\varepsilon_m - \hat{\varepsilon}_m) \\ &\quad + S(t)(\boldsymbol{W}^* - \boldsymbol{W})\boldsymbol{\phi} \\ &\quad - \frac{1}{\eta_1}(\varepsilon_m - \hat{\varepsilon}_m)\dot{\hat{\varepsilon}}_m - \frac{1}{\eta_2}(\boldsymbol{W}^* - \boldsymbol{W})\boldsymbol{F}^{-1}\dot{\boldsymbol{W}}^T \\ &= -(\lambda + C)\xi_1^2(t) - S(t)Ksign(S) + S(t)(\varepsilon_m - \hat{\varepsilon}_m) \\ &\quad + S(t)(\boldsymbol{W}^* - \boldsymbol{W})\boldsymbol{\phi} - S(t)(\varepsilon_m - \hat{\varepsilon}_m) - S(t)(\boldsymbol{W}^* - \boldsymbol{W})\boldsymbol{\phi} \\ &= -(\lambda + C)\xi_1^2(t) - S(t)Ksign(S) \\ &= -(\lambda + C)\xi_1^2(t) - K\,|S(t)| \leq 0\end{aligned} \tag{37}$$

Thereby, it can be observed that V_3 is positive definite while its time derivative is negative definite. When $|S(t)|$ tends to infinity, V_3 approaches to infinity. According to the Lyapunov stability criterion [43], the closed-loop controller is globally asymptotically stable, and the admittance error $\xi_1(t)$ gradually converges to zero and approaches the sliding surface $S(t) = 0$ in finite time. This completes the proof of the system stability.

III. EXPERIMENTAL PROTOCOL

A. Subjects and Experimental Setup

In this research, we focused on validating the performance of the proposed ABSMCNN scheme on four neurologically intact healthy subjects and four stroke patients with different degrees of hemiplegia. Table II presents the anthropometry parameters and Fugl-Meyer assessment score [44] of each subjects. The experimental protocol includes two separate tests, i.e. the repetitively trajectory tracking test with different admittance parameters and the human-robot cooperative resistive training test with adaptive interaction compliance. The ethical approval of experimental study was obtained from the Institutional Review Board of Nanjing University of Aeronautics and Astronautics under the protocol IRB [2022]-178. Before the experimental protocol was carried out, all participants received a detailed explanation on the potential risks of experiments and signed an informed consent prior to their participation in this study. In addition, all subjects gave us the authority to utilize their personal information and experimental results.

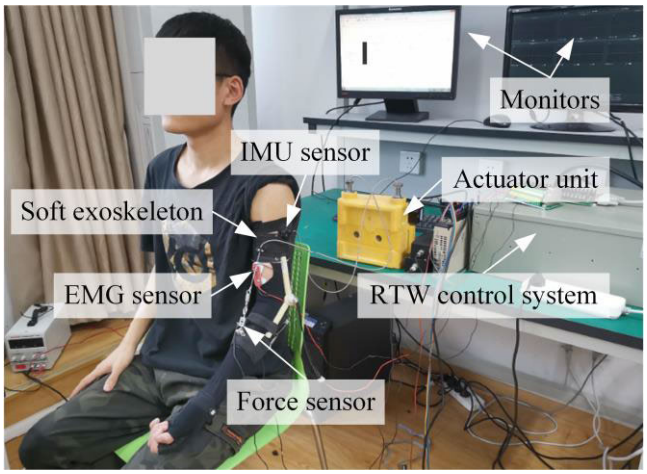

Fig. 5. The experimental setup and soft elbow rehabilitation exoskeleton prototype worn by a participant.

The verification experiments were conducted on the aforementioned soft elbow rehabilitation exoskeleton and real-time control system, as shown in Fig. 2. The experimental setup and exoskeleton prototype worn by a participant is shown in Fig. 5. The participants were instructed to comfortably sit down on a chair and wear the soft elbow exoskeleton with the help of a laboratory assistant. The monitors of host computer and follower computer were utilized to displace the status of program execution and the guidance information for visual feedback. All participants were required to repeat the compliance-varying repetitively trajectory tracking test and adaptive cooperative resistive training test six times for each condition. There was a ten-minute break between each experiment to keep participant relaxed and prevent muscle fatigue.

B. Repetitively Trajectory Tracking Test With Different Admittance Parameters

Firstly, the repetitively trajectory tracking test with different admittance parameters was conducted, with the aim of investigating the performance and feasibility of the proposed control strategy in providing rigid passive training assistance and compliant passive training assistance. For the severe hemiplegia patients seriously lacking of muscle contraction and movement ability, the repetitively rigid passive training along rational trajectory contributes to improving muscle contraction function and eliminating articular spasm. In this case, the control purpose focuses on guaranteeing the trajectory tracking accuracy during training, and the patients remain in completely passive state. On the other side, if the hemiplegia patients have turned better and recovered partial motor functions, the repetitively compliant trajectory tracking training test combined with admittance regulation can induce the active participation of patients and, furthermore, modulate the actual training trajectory based on the human elbow joint torque from patient. It is conducive to enhancing the compliance, immersion and comfort during rehabilitation training.

In the repetitively rigid passive training test, the adaptive factor was set to γ =0. The control parameters of the

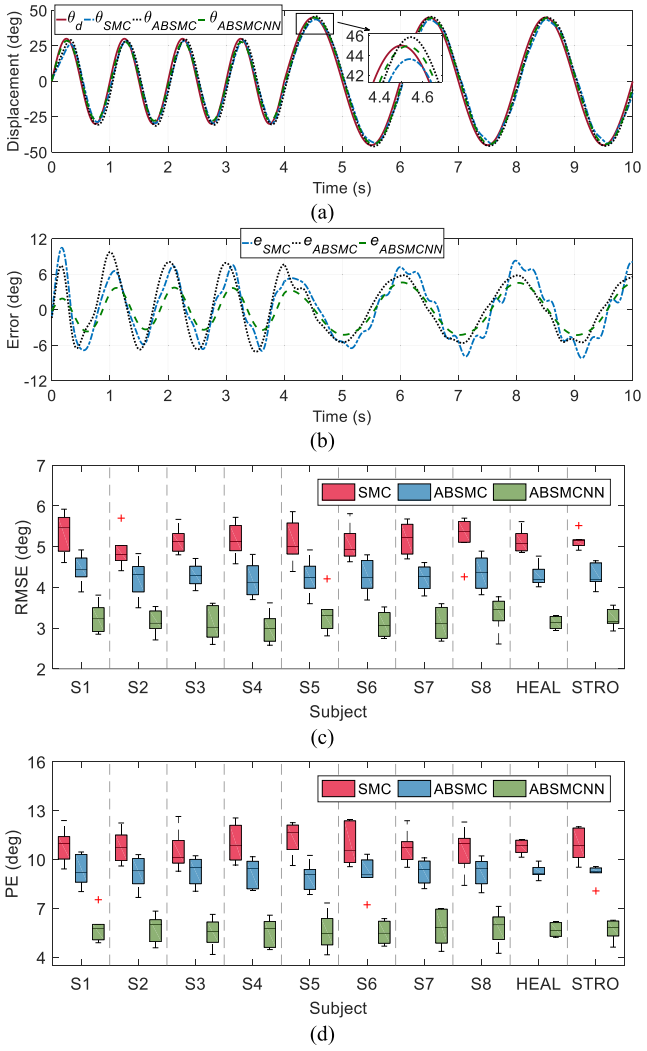

Fig. 6. The results of repetitively rigid passive training experiment. (a) The comparison among the desired trajectory and the actual trajectories with different control strategies conducted by S1. (b) The comparison of the actual joint angle errors with different control strategies conducted by S1. (c) The statistical results of the RMSE of different participants and different control strategies. Here, HEAL denotes the statistical results of all healthy participants, STRO denotes the statistical results of all stroke participants. (d) The statistical results of the PE of different participants and different control strategies.

inner-loop adaptive backstepping sliding mode controller were careful selected via trial and error in order to ensure position tracking accuracy and system stability, and the control parameters were set to λ =0.83, $C = 0.37$, $K = 3.5$, η_1 =5.5 and η_1 =4.1. In this test, the participants were commanded to passively perform repetitive rehabilitation training with the assistance of exoskeleton. The duration of each trial was set to 10 s. The desired trajectory of elbow joint was defined as a sinusoid wave trajectory, wherein the first 4 s saw an amplitude of 30° and a frequency of 1 Hz, which then changed to 45° and 0.5 Hz from the moment $t = 4$ s to $t = 10$ s. The desired trajectory can be seen in Fig. 6(a).

Meanwhile, in the repetitively compliant trajectory tracking training test, the adaptive factor was set to $\gamma = 2$. The parameters of admittance model (i.e. inertial gain, damping gain, and stiffness gain) were set to three groups (i.e. high admittance: $M_d = 0.2$, $B_d = 0.2$, $K_d = 0.2$; middle admittance: $M_d = 0.1$, $B_d = 0.1$, $K_d = 0.1$; low admittance: $M_d = 0.05$, $B_d = 0.05$, $K_d = 0.05$). The participants were commanded to wittingly generate biological elbow joint torque and adjust the actual training trajectory with their active intention. The duration of each trial was set to 20 s. The desired trajectory of elbow joint was defined as a sinusoid wave trajectory with an amplitude of 45° and a frequency of 0.5 Hz. The desired trajectory is shown in Fig. 7(a).

To quantitatively evaluate the control performance, the root mean square error (RMSE), the peak error (PE), and the active cooperation level (ACL) are defined as follows:

$$\mathrm{RMSE} = \sqrt{\frac{1}{\omega}\sum_{i=1}^{\omega} e_i^2} \tag{38}$$

$$\mathrm{PE} = \max|e_i| \tag{39}$$

$$\mathrm{ACL} = \sqrt{\sum_{i=1}^{\omega} e_i^2 \Big/ \sum_{i=1}^{\omega} \tau_{h\_i}^2} \tag{40}$$

where e_i and τ_{h_i} represent the ith data of joint angle error and elbow joint torque, ω denotes the total number of data.

C. Cooperative Resistive Training Test With Adaptive Interaction Compliance

Secondly, the cooperative resistive training test integrated with self-adaptive interaction compliance and active motion intention of patients was carried out, with the aim of evaluating the effectiveness of the ABSMCNN control strategy in assisting elbow flexion-extension training in active-training mode, assist-as-needed training mode, and safety training mode. For the slight hemiplegia patients who have recovered most of the motor function, motion intention-based cooperative resistive training is beneficial to enhancing the rehabilitation treatment efficiency and recovering psychological confidence. In this case, the control purpose focuses on allowing the active training of patients and adjusting human-robot interaction compliance in different work areas based on practical training requirements.

In the cooperative resistive training test, the adaptive factor is modulated according to the actual joint angle error and the selected parameters of different training modes. The predefined maximum adaptive factor was set to $\gamma_{\max}$ =4. The boundaries of different work areas were set to R_a =15 mm, R_n = 35 mm. The constants defined to adjust the variation rate of interaction compliance are set to $P = 2$, $L = 10$. The duration of each trial was set to 25 s. The desired trajectory of elbow joint was set to follow a point-to-point polyline trajectory with six waypoints as follows: $\mathrm{P_a}$ = (0 s, 0°), $\mathrm{P_b}$ = (2 s, 45°), $\mathrm{P_c}$ = (6 s, -60°), $\mathrm{P_d}$ = (14 s, 60°), $\mathrm{P_e}$ = (22 s, −45°), $\mathrm{P_f}$ = (25 s, 0°). The desired trajectory can be seen in Fig. 8(a). The parameters of admittance model were set to the high admittance level. The experimenters needed to actively execute reciprocating elbow flexion/extension training on the sagittal plane. A training guidance module was

developed in the low-level follower computer, which can immerse the experimenters into the virtual world and guide

them to actively follow the planning trajectory during cooperative resistive rehabilitation training. From (10) and (13), the interaction torque applied by wearer can be mapped into the desired elbow joint angle adjustment, which leads to the active elbow motion toward the corresponding direction. The resistive torque from the soft exoskeleton can impede the intention-based free motion of human elbow and, as a result, adjust rehabilitation training intensity.

IV. Results and Discussion

Fig. 6 presents the results of the repetitively rigid passive training test. To evaluate the position control performance of the inner-loop of proposed ABSMCNN control strategy, the experimental results were compared to those of a conventional sliding mode controller (SMC) [45]. Furthermore, to validate the effectiveness of the developed neural network-based disturbance compensation method, the ABSMCNN without neural network compensation (ABSMC) was also applied in the comparative experiments. Fig 6 (a) gives the comparison results of the desired trajectory and the actual trajectories with different control strategies conducted by subject S1 in one trial. The actual joint angle errors are compared in Fig 6 (b). Besides, on the left side of Fig 6 (c) and Fig 6 (d), the statistical results of the RMSE and PE of each participant using different control strategies are summarized. The statistical results of all healthy and all stroke participants are compared on the right side of Fig 6 (c) and Fig 6 (d). All participants carried out the repetitively rigid passive training test six times for each control strategy.

According to the results in Fig 6, it can be clearly observed that the position control accuracy of proposed ABSMCNN scheme is higher than those of SMC and ABSMC. More specifically, it can be calculated that the average RMSE of all eight participants and six trials with ABSMCNN is 3.18°, which is lower than those of SMC (i.e., 5.15°) and ABSMC (i.e., 4.30°). Similarly, the proposed ABSMCNN achieved the lowest average PE (i.e., 5.68°) when compared with those of the SMC (i.e., 10.85°) and ABSMC (i.e., 9.19°). Therefore, the trajectory tracking error significantly decreases when the neural-network-based adaptive admittance backstepping sliding mode control strategy is applied. The neural network compensation scheme contributes to a decrease of 26.05% in average RMSE and a decrease of 38.19% in average PE. Furthermore, the Kruskal-Wallis statistical significance tests [46] with a significance level of α =0.05 were applied to analyze the experimental results and reveal the statistically significant differences. It can be calculated that the p-value of RMSE for different control strategies, participants and trials is 0.0073 ($p < 0.05$). Meanwhile, the p-value of PE for different control strategies, participants and trials is 0.0061 ($p < 0.05$). Moreover, a Bonferroni pairwise post-hoc analysis [47] was performed to prove the significant differences between two groups. Then, the significant post-hoc pairwise differences were found between ABSMCNN and SMC (p-value of RMSE: 0.0173, p-value of PE: 0.0135), as well as between ABSMCNN and ABSMC (p-value of RMSE: 0.0156, p-value of PE: 0.0129). The results indicates that the differences of trajectory tracking performance using different methods are of statistical significance.

On the other side, the average results on two categories of healthy and stroke participants with different control strategies were compared. Here, the average RMSE of healthy subjects (i.e., SMC: 5.11 °, ABSMC: 4.34 °, ABSMCNN: 3.13 °) are correspondingly similar to those of stroke subjects (i.e., SMC: 5.20°, ABSMC: 4.27 °, ABSMCNN: 3.23 °). The average PE of healthy participants (i.e., SMC: 10.78 °, ABSMC: 9.25 °, ABSMCNN: 5.63 °) are similar to those of stroke subjects (i.e., SMC: 10.91 °, ABSMC: 9.14 °, ABSMCNN: 5.72 °).

Thus, the experimental results demonstrate the superiority of ABSMCNN over SMC and ABSMC in improving the position control accuracy of repetitively rigid passive training. Besides, the variations of motor functions of different subjects almost have no influence on the trajectory tracking accuracy. Moreover, the ABSMCNN scheme also presents an advantage in accuracy when compared with other trajectory tracking control methods of soft exoskeleton. For example, a hierarchical cascade control strategy proposed in [48] for soft arm exoskeleton achieves a

PE about 8.92 °, which is higher than that of ABSMCNN. In [17], a two-layer controller combined with bang-bang control and PID control was developed for a textile-based soft upper-limb exoskeleton, and its average RMSE in trajectory tracking test (about 6 °) is higher than that of ABSMCNN.

The experimental results of repetitively compliant trajectory tracking training test are shown in Fig. 7. The proposed ABSMCNN was applied in this experiment and the parameters of admittance model were set to high admittance, middle admittance and low admittance respectively. More specifically, Fig 7 (a) presents the comparison of the desired trajectory and the actual trajectories with different admittance parameters conducted by subject S1 in one trial, when the subject produces the voluntary effort. Fig 7 (b) gives the time histories of the corresponding actual joint angle errors with different admittance parameters. The envelope of sEMG signals from the triceps and biceps of S1 in the tests with high admittance, middle admittance and low admittance are illustrated in Figs 7 (c)-7 (e). The time histories of the estimated elbow joint torques during experiment are given in Fig 7 (f). It can be found that the deviation between desired elbow trajectory and actual elbow trajectory shows positive correlation with the strength of sEMG signals and the elbow joint torque generated by wearer. The amplitudes of the sEMG signals from triceps and biceps, which have been amplified and filtered, were all limited within the range of −300 mV to 300 mV. Correspondingly, the applied elbow joint torque was changed within the range of −5 Nm to 9 Nm. The magnitude and direction of the joint angle errors are consistent with the applied joint torque. More specifically, it can be calculated that the RMSE and PE of the experiment with low admittance are 24.13° and 50.86°, which are higher than those with middle admittance (RMSE:13.98°, PE: 29.66°) and high admittance (RMSE: 9.41°, PE: 22.13°). It indicates that there is an upward trend of joint angle error with the decrease of admittance parameters.

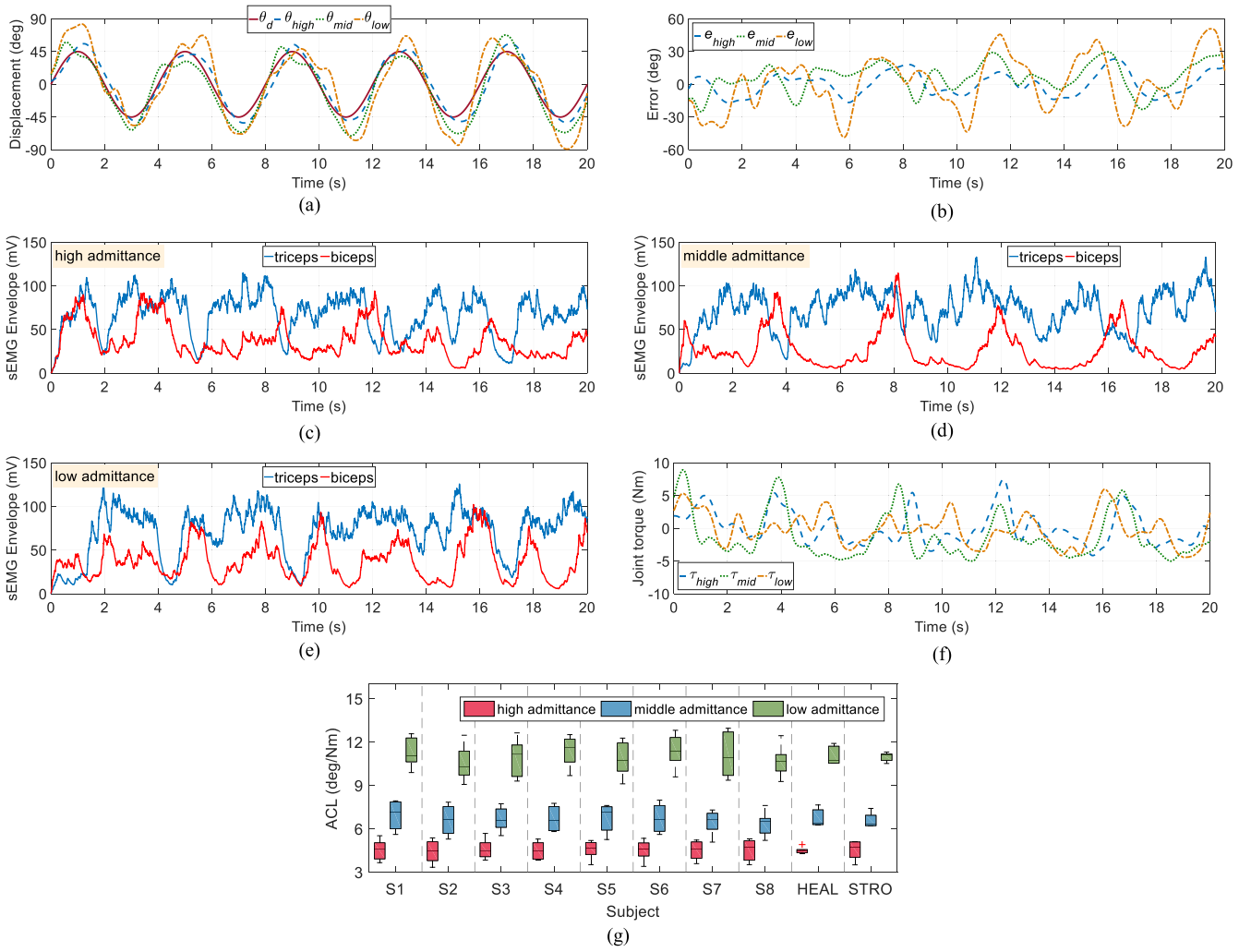

Fig. 7. The results of repetitively compliant trajectory tracking training experiment. (a) The comparison among the desired trajectory and the actual trajectories with different admittance parameters conducted by S1. (b) The comparison of the actual joint angle errors with different admittance parameters conducted by S1. (c) ∼ (e) The envelope of sEMG signals from triceps and biceps in the tests with high admittance, middle admittance and low admittance. (f) The estimated elbow joint torque of S1. (g) The statistical results of the ACL of different participants and different admittance parameters. Here, HEAL denotes the statistical results of all healthy participants, STRO denotes the statistical results of all stroke participants.

The statistical results of the ACL of each participant adopting different admittance parameters are summarized on the left side of Fig 7 (g). Meanwhile, the statistical results of all healthy and stroke participants are compared on the right side of Fig 7 (g). All the participants carried out the repetitively compliant trajectory tracking test six times for each admittance level. It can be obtained that the average ACL of all eight participants and six trials with high admittance is 4.51 °/Nm, which is lower than those with middle admittance (6.63 °/Nm) and low admittance (10.99 °/Nm). Besides, the average ACL of healthy and stroke participants were analyzed. The average ACL of healthy participants with different admittance levels (i.e., high admittance: 4.46 °/Nm, middle admittance: 6.72 °/Nm, low admittance: 11.13 °/Nm) are correspondingly similar to those of stroke participants (i.e., high admittance: 4.56 °/Nm, middle admittance: 6.54 °/Nm, low admittance: 10.85 °/Nm). The Kruskal-Wallis tests were applied to reveal the statistically significant differences among the results with high admittance, middle admittance and low admittance. It can be calculated that the p-value of ACL for different admittance levels, participants. and trials is 0.0039 ($p < 0.05$), which indicates that the differences of ACL using different admittance parameters are of statistical significance.

Therefore, the experimental results verify that the active joint torque generate by participant can realize real-time adaption of the practical training trajectory, and the human-exoskeleton interaction compliance level increases with the decrease of admittance parameters. In addition, the variations of motor functions and hemiplegia degrees almost have no influence on the value of ACL. Compared with the existing passive tracking control schemes without trajectory regulation [20], [22] and the compliance tracking control strategies with constant interaction characteristics [49], the proposed ABSMCNN scheme shows superiority in helping patients induce their active participation during repetitively trajectory tracking rehabilitation training.

Fig. 8 gives the results of cooperative resistive training test with adaptive interaction compliance. More specifically,

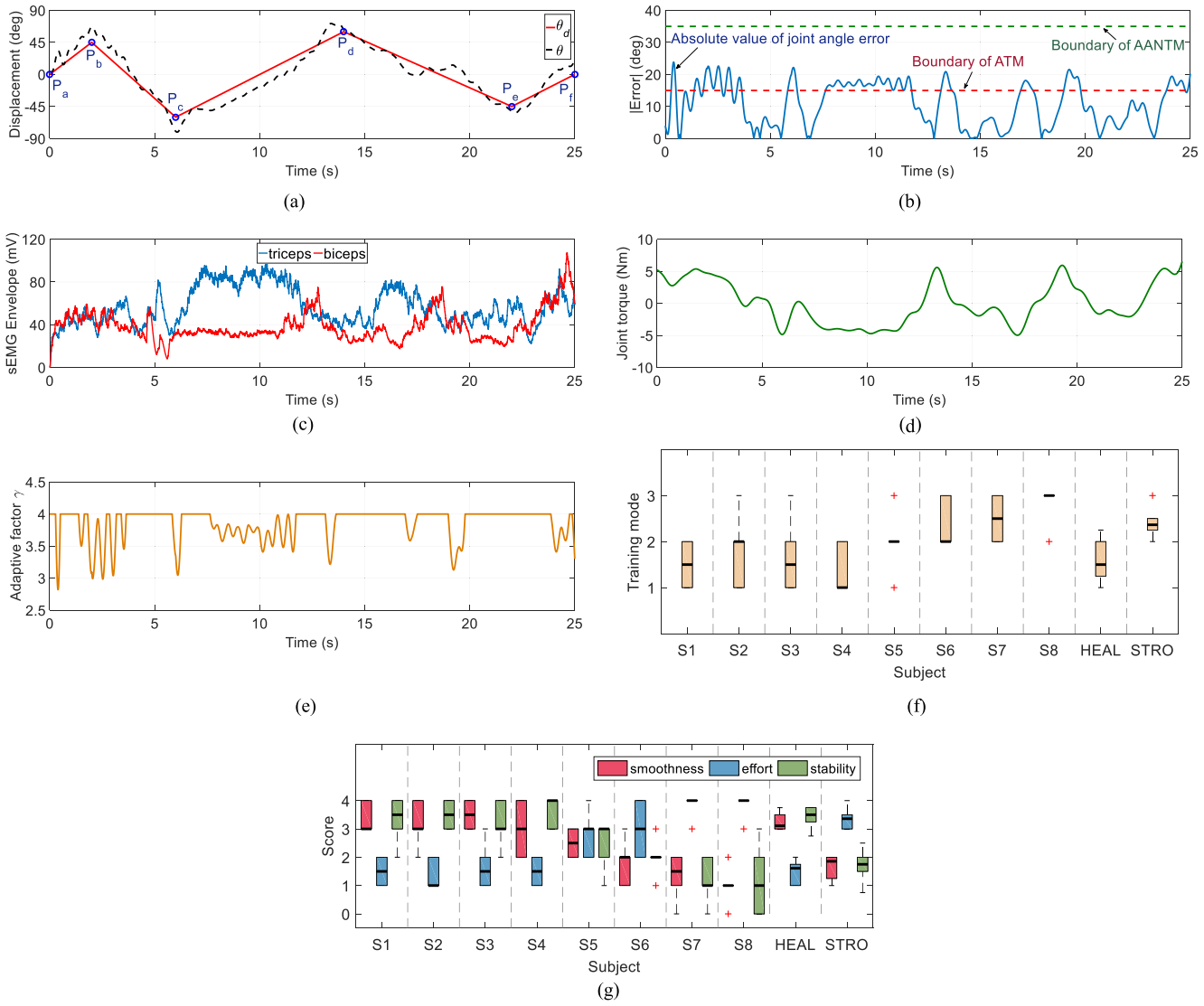

Fig. 8. The results of cooperative resistive training experiment with adaptive interaction compliance. (a) The comparison between the desired trajectory and the actual trajectory of S1. (b) The absolute value of actual joint angle error of S1 and the boundaries of ATM and AANTM. (c) The envelope of sEMG signals from triceps and biceps. (d) The estimated elbow joint torque of S1. (e) The variation of adaptive factor γ. (f) The statistical results of the number of activated training modes of different participants. HEAL denotes the statistical results of all healthy participants, STRO is the statistical results of all stroke participants. g) The statistical questionnaire results related to the smoothness, effort and stability of experiments conducted by different participants.

Fig. 8(a) shows the comparison between the desired training trajectory and actual training trajectory of the experiment conducted by subject S1 in one trial. The time histories of the absolute value of actual joint angle errors and the boundaries of ATM and AANTM are shown in Fig. 8(b). It can be found that the cooperative resistive training with predefined waypoints can be completed via the proposed ABSMCNN scheme. In the trial with S1, the training mode is switched between ATM and AANTM for many times. Due to the need to adapt to the cooperative resistive training process, the switching frequency in initial period is higher than those in the middle and later periods. The time histories of the envelope of sEMG signals from the triceps and biceps and the corresponding estimated elbow joint torques are shown in Figs. 8(c) and 8(d). We can observe that the actual training trajectory is modulated according to the sEMG signals and elbow joint torques, and that allows the participant to actively dominate the rehabilitation training based on their own motion intention. The time histories of the position error-based adaptive factor γ is given in Fig. 8(e). It can be seen that the adaptive factor in the ATM is equal to 4. Meanwhile, in the AANTM, the adaptive factor decreases rapidly with the increase of joint angle errors, contributing to reducing interaction compliance and ensuring training integrity.

The statistical results of the number of activated training modes (i.e., 1, 2 and 3) of all eight participants in six trials are summarized in Fig. 8(f). Moreover, the statistical results of all healthy participants and all stroke participants are compared. Here, 1 denotes the training in ATM; 2 denotes the training in AANTM; 3 denotes the training in STM. The average value of activated training mode number of healthy participants is 1.58, while the average value of activated training mode

number of stroke participants is 2.42. It can be seen that the average activated training mode number increases with the paralysis degree of participant. The training modes of healthy participants are mainly distributed in the ATM and AANTM regions, as they have enough muscular strength to complete training. By contrast, for the stroke patients, the training modes are mainly distributed in the AANTM and STM regions. Especially, the patient with severe paralysis basically worked in the STM due to the lack of motor ability. It conduces to guarantee that the disabled subjects can fulfill the training task with robot assistance and avoid safety problems. Moreover, the Kruskal-Wallis tests were applied to reveal the statistically significant differences of activated training mode of the participants with different motor functions. It can be calculated that the p-value of training mode is 0.0126 ($p < 0.05$), which indicates that the differences are of statistical significance. Most of the existing cooperative control schemes of soft exoskeletons were developed with a single rehabilitation training mode [31], [50], [51]. Compared with them, the proposed ABSMCNN with four training modes shows superiority in satisfying the training requirements of patients with different hemiplegia degrees and different training objectives.

A questionnaire study about the smoothness, effort and stability of each trial for all participants were conducted to evaluate the human-exoskeleton collaboration performance [52]. The performance scores was defined as five levels, i.e., 0, 1, 2, 3 and 4. Here, 0 represents the worst performance, while 4 represents the best performance. In Fig. 8(g), the statistical questionnaire results of the cooperative resistive rehabilitation training experiment conducted by different participants in six trials are summarized. Besides, the statistical results of healthy participants and stroke participants are compared and illustrated. It can be calculated that, for the healthy participants, the average smoothness score is 3.25, the average effort score is 1.50 and the average stability score is 3.42. Meanwhile, for the stroke participants, the average smoothness score is 1.67, the average effort score is 3.38 and the average stability score is 1.71. The Kruskal-Wallis tests were applied to see the statistically significant differences between the results of healthy and stroke subjects. The p-value of smoothness score, effort score and stability score are 0.0159, 0.0182 and 0.0141, respectively. They are all smaller than 0.05, indicating that the differences are significant. We can observe that the smoothness scores and stability scores of stroke patients are lower than those of the healthy subjects. That is mainly caused by the variation of adaptive factor in AANTM and STM, leading to the rapid adjustment of planning trajectory. In addition, the participants with severe paralysis and moderate paralysis found that they needed more effort to complete the cooperative resistive training when compared with the healthy subjects and the patients with slight paralysis.

V. Conclusion and Future Works

In this research, a new ABSMCNN control strategy was proposed for a soft elbow exoskeleton to assist multi-mode cooperative rehabilitation training. The human-robot coupling dynamic model was developed based on a sEMG-based joint torque estimation method and a neural network-based disturbance observer. The interaction characteristics of ABSMCNN is modulated via an adaptive admittance model according to real-time position errors, and it can be transformed into PTM, ATM, AANTM and STM to meet the specific therapy requirements. It contributes to inducing the active participation of patients and ensuring the accomplishment and safety of training. The effectiveness of proposed scheme was evaluated via the compliant trajectory tracking test and the adaptive cooperative resistive training test conducted by four healthy subjects and four stroke patients. Experimental results involving position control accuracy, active cooperation level, smoothness, effort and stability were analyzed and discussed.

Our future works will cover various areas. For structure design, we plan to optimize the wearable components and actuator module, so that the wearable comfort and lightweight level can be promoted. For control methodology, the adaptive law of admittance model will be improved according to the clinical knowledge of therapists. For rehabilitation evaluation, a visual recovery evaluation system will be developed for the quantitative analysis of therapy effect and optimization of rehabilitation strategy.

References

[1] World Health Organization. *Stroke, Cerebrovascular Accident: Health Topics*. Accessed: Jan. 24, 2023. [Online]. Available: http://www.emro.who.int/health-topics/stroke-cerebrovascular-accident

[2] R. L. Hybart and D. P. Ferris, "Embodiment for robotic lower-limb exoskeletons: A narrative review," *IEEE Trans. Neural Syst. Rehabil. Eng.*, vol. 31, pp. 657–668, 2023.

[3] N. Sun, G. Li, and L. Cheng, "Design and validation of a self-aligning index finger exoskeleton for post-stroke rehabilitation," *IEEE Trans. Neural Syst. Rehabil. Eng.*, vol. 29, pp. 1513–1523, 2021.

[4] E. Peperoni et al., "Self-aligning finger exoskeleton for the mobilization of the metacarpophalangeal joint," *IEEE Trans. Neural Syst. Rehabil. Eng.*, vol. 31, pp. 884–894, 2023.

[5] Y. Qian, H. Yu, and C. Fu, "Adaptive oscillator-based assistive torque control for gait asymmetry correction with a nSEA-driven hip exoskeleton," *IEEE Trans. Neural Syst. Rehabil. Eng.*, vol. 30, pp. 2906–2915, 2022.

[6] Y. Tu, A. Zhu, J. Song, X. Zhang, and G. Cao, "Design and experimental evaluation of a lower-limb exoskeleton for assisting workers with motorized tuning of squat heights," *IEEE Trans. Neural Syst. Rehabil. Eng.*, vol. 30, pp. 184–193, 2022.

[7] C. G. Mcdonald, B. J. Fregly, and M. K. O'Malley, "Effect of robotic exoskeleton motion constraints on upper limb muscle synergies: A case study," *IEEE Trans. Neural Syst. Rehabil. Eng.*, vol. 29, pp. 2086–2095, 2021.

[8] Y. Zhu, Q. Wu, B. Chen, D. Xu, and Z. Shao, "Design and evaluation of a novel torque-controllable variable stiffness actuator with reconfigurability," *IEEE/ASME Trans. Mechatronics*, vol. 27, no. 1, pp. 292–303, Feb. 2022.

[9] F. Patané, S. Rossi, F. Del Sette, J. Taborri, and P. Cappa, "WAKE-up exoskeleton to assist children with cerebral palsy: Design and preliminary evaluation in level walking," *IEEE Trans. Neural Syst. Rehabil. Eng.*, vol. 25, no. 7, pp. 906–916, Jul. 2017.

[10] N. Vitiello et al., "NEUROExos: A powered elbow exoskeleton for physical rehabilitation," *IEEE Trans. Robot.*, vol. 29, no. 1, pp. 220–235, Feb. 2013.

[11] A. T. Asbeck, S. M. M. De Rossi, I. Galiana, Y. Ding, and C. J. Walsh, "Stronger, smarter, softer: Next-generation wearable robots," *IEEE Robot. Autom. Mag.*, vol. 21, no. 4, pp. 22–33, Dec. 2014.

[12] Q. Chen, S. Guo, J. Wang, J. Wang, D. Zhang, and S. Jin, "Biomechanical and physiological evaluation of biologically-inspired hip assistance with belt-type soft exosuits," *IEEE Trans. Neural Syst. Rehabil. Eng.*, vol. 30, pp. 2802–2814, 2022.

[13] M. Xiloyannis et al., "Soft robotic suits: State of the art, core technologies, and open challenges," *IEEE Trans. Robot.*, vol. 38, no. 3, pp. 1343–1362, Jun. 2022.

[14] Y. Zhang et al., "Soft exoskeleton mimics human cough for assisting the expectoration capability of SCI patients," *IEEE Trans. Neural Syst. Rehabil. Eng.*, vol. 30, pp. 936–946, 2022.

[15] X. Tan, B. Zhang, G. Liu, X. Zhao, and Y. Zhao, "Cadence-insensitive soft exoskeleton design with adaptive gait state detection and iterative force control," *IEEE Trans. Autom. Sci. Eng.*, vol. 19, no. 3, pp. 2108–2121, Jul. 2022.

[16] M. K. Burns, D. Pei, and R. Vinjamuri, "Myoelectric control of a soft hand exoskeleton using kinematic synergies," *IEEE Trans. Biomed. Circuits Syst.*, vol. 13, no. 6, pp. 1351–1361, Dec. 2019.

[17] T. Proietti et al., "Sensing and control of a multi-joint soft wearable robot for upper-limb assistance and rehabilitation," *IEEE Robot. Autom. Lett.*, vol. 6, no. 2, pp. 2381–2388, Apr. 2021.

[18] M. Hosseini, R. Meattini, A. San-Millan, G. Palli, C. Melchiorri, and J. Paik, "A sEMG-driven soft ExoSuit based on twisted string actuators for elbow assistive applications," *IEEE Robot. Autom. Lett.*, vol. 5, no. 3, pp. 4094–4101, Jul. 2020.

[19] W. M. A. Rosado, L. G. V. Valdés, A. B. Ortega, J. R. Ascencio, and C. D. G. Beltrán, "Passive rehabilitation exercises with an ankle rehabilitation prototype based in a robot parallel structure," *IEEE Latin Amer. Trans.*, vol. 15, no. 1, pp. 48–56, Jan. 2017.

[20] Q. Wu, B. Chen, and H. Wu, "RBFN-based adaptive backstepping sliding mode control of an upper-limb exoskeleton with dynamic uncertainties," *IEEE Access*, vol. 7, pp. 134635–134646, 2019.

[21] B. Brahmi, M. Saad, C. Ochoa-Luna, M. H. Rahman, and A. Brahmi, "Adaptive tracking control of an exoskeleton robot with uncertain dynamics based on estimated time-delay control," *IEEE/ASME Trans. Mechatronics*, vol. 23, no. 2, pp. 575–585, Apr. 2018.

[22] A. Riani, T. Madani, A. Benallegue, and K. Djouani, "Adaptive integral terminal sliding mode control for upper-limb rehabilitation exoskeleton," *Control Eng. Pract.*, vol. 75, pp. 108–117, Jun. 2018.

[23] S. Han, H. Wang, Y. Tian, and N. Christov, "Time-delay estimation based computed torque control with robust adaptive RBF neural network compensator for a rehabilitation exoskeleton," *ISA Trans.*, vol. 97, pp. 171–181, Feb. 2020.

[24] Q. Wu and Y. Chen, "Development of an intention-based adaptive neural cooperative control strategy for upper-limb robotic rehabilitation," *IEEE Robot. Autom. Lett.*, vol. 6, no. 2, pp. 335–342, Apr. 2021.

[25] F. S. di Luzio et al., "Bio-cooperative approach for the human-in-the-loop control of an end-effector rehabilitation robot," *Frontiers Neurorobotics*, vol. 12, p. 67, Oct. 2018.

[26] C. Chen, S. Zhang, X. Zhu, J. Shen, and Z. Xu, "Disturbance observer-based patient-cooperative control of a lower extremity rehabilitation exoskeleton," *Int. J. Precis. Eng. Manuf.*, vol. 21, no. 5, pp. 957–968, May 2020.

[27] H. J. Asl, K. Katagiri, T. Narikiyo, M. Yamashita, and M. Kawanishi, "Satisfying task completion and assist-as-needed performance in robotic exoskeletons," *IEEE Trans. Med. Robot. Bionics*, vol. 3, no. 3, pp. 791–800, Aug. 2021.

[28] A. U. Pehlivan, D. P. Losey, and M. K. O'Malley, "Minimal assist-as-needed controller for upper limb robotic rehabilitation," *IEEE Trans. Robot.*, vol. 32, no. 1, pp. 113–124, Feb. 2016.

[29] Q. Wu, X. Wang, B. Chen, and H. Wu, "Development of a minimal-intervention-based admittance control strategy for upper extremity rehabilitation exoskeleton," *IEEE Trans. Syst., Man, Cybern., Syst.*, vol. 48, no. 6, pp. 1005–1016, Jun. 2018.

[30] A. Morbi, M. Ahmadi, A. D. C. Chan, and R. Langlois, "Stability-guaranteed assist-as-needed controller for powered orthoses," *IEEE Trans. Control Syst. Technol.*, vol. 22, no. 2, pp. 745–752, Mar. 2014.

[31] A. F. Pérez Vidal et al., "Soft exoskeletons: Development, requirements, and challenges of the last decade," *Actuators*, vol. 10, no. 7, p. 166, Jul. 2021.

[32] M. Xiloyannis et al., "Design and validation of a modular one-to-many actuator for a soft wearable exosuit," *Frontiers Neurorob.*, vol. 13, p. 39, Jun. 2019.

[33] Q. Chen, S. Guo, L. Sun, Q. Liu, and S. Jin, "Inertial measurement unit-based optimization control of a soft exosuit for hip extension and flexion assistance," *J. Mech. Robot.*, vol. 13, no. 2, Apr. 2021, Art. no. 021016.

[34] R. Ismail et al., "Soft elbow exoskeleton for upper limb assistance incorporating dual motor-tendon actuator," *Electronics*, vol. 8, no. 10, p. 1184, Oct. 2019.

[35] C. Siviy et al., "Offline assistance optimization of a soft exosuit for augmenting ankle power of stroke survivors during walking," *IEEE Robot. Autom. Lett.*, vol. 5, no. 2, pp. 828–835, Apr. 2020.

[36] Z. Shao, Q. Wu, B. Chen, H. Wu, and Y. Zhang, "Modeling and inverse control of a compliant single-tendon-sheath artificial tendon actuator with bending angle compensation," *Mechatronics*, vol. 63, Nov. 2019, Art. no. 102262.

[37] Q. Wu and Y. Chen, "Adaptive cooperative control of a soft elbow rehabilitation exoskeleton based on improved joint torque estimation," *Mech. Syst. Signal Process.*, vol. 184, Feb. 2023, Art. no. 109748.

[38] N. Sun et al., "Continuous estimation of human knee joint angles by fusing kinematic and myoelectric signals," *IEEE Trans. Neural Syst. Rehabil. Eng.*, vol. 30, pp. 2446–2455, 2022.

[39] M. M. Rayguru, R. E. Mohan, R. Parween, L. Yi, A. V. Le, and S. Roy, "An output feedback based robust saturated controller design for pavement sweeping self-reconfigurable robot," *IEEE/ASME Trans. Mechatronics*, vol. 26, no. 3, pp. 1236–1247, Jun. 2021.

[40] Y. Zhu, Q. Wu, B. Chen, Z. Zhao, and C. Liang, "Physical human–robot interaction control of variable stiffness exoskeleton with sEMG-based torque estimation," *IEEE Trans. Ind. Informat.*, vol. 19, no. 10, pp. 10601–10612, Oct. 2023, doi: 10.1109/TII.2023.3240749.

[41] L. Lu, Q. Wu, X. Chen, Z. Shao, B. Chen, and H. Wu, "Development of a sEMG-based torque estimation control strategy for a soft elbow exoskeleton," *Robot. Auto. Syst.*, vol. 111, pp. 88–98, Jan. 2019.

[42] Z. Li, B. Wang, F. Sun, C. Yang, Q. Xie, and W. Zhang, "SEMG-based joint force control for an upper-limb power-assist exoskeleton robot," *IEEE J. Biomed. Health Informat.*, vol. 18, no. 3, pp. 1043–1050, May 2014.

[43] M. Zhang, J. Huang, Y. Cao, C.-H. Xiong, and S. Mohammed, "Echo state network-enhanced super-twisting control of passive gait training exoskeleton driven by pneumatic muscles," *IEEE/ASME Trans. Mechatronics*, vol. 27, no. 6, pp. 5107–5118, Dec. 2022.

[44] D. J. Gladstone, C. J. Danells, and S. E. Black, "The Fugl–Meyer assessment of motor recovery after stroke: A critical review of its measurement properties," *Neurorehabilitation Neural Repair*, vol. 16, no. 3, pp. 232–240, Sep. 2002.

[45] M. Babaiasl, S. N. Goldar, M. H. Barhaghtalab, and V. Meigoli, "Sliding mode control of an exoskeleton robot for use in upper-limb rehabilitation," in *Proc. 3rd RSI Int. Conf. Robot. Mechatronics (ICROM)*, Oct. 2015, pp. 694–701.

[46] Y. Chan et al., "Learning and understanding the Kruskal–Wallis one-way analysis-of-variance-by-ranks test for differences among three or more independent groups," *Phys Ther*, vol. 77, no. 12, pp. 1755–1762, 1997.

[47] S. Lalwani, R. Kumar, and N. Gupta, "A novel two-level particle swarm optimization approach for efficient multiple sequence alignment," *Memetic Comput.*, vol. 7, no. 2, pp. 119–133, Jun. 2015.

[48] B. K. Dinh, M. Xiloyannis, C. W. Antuvan, L. Cappello, and L. Masia, "Hierarchical cascade controller for assistance modulation in a soft wearable arm exoskeleton," *IEEE Robot. Autom. Lett.*, vol. 2, no. 3, pp. 1786–1793, Jul. 2017.

[49] C. R. Carignan, M. P. Naylor, and S. N. Roderick, "Controlling shoulder impedance in a rehabilitation arm exoskeleton," in *Proc. IEEE Int. Conf. Robot. Autom.*, May 2008, pp. 2453–2458.

[50] M. Li et al., "An attention-controlled hand exoskeleton for the rehabilitation of finger extension and flexion using a rigid-soft combined mechanism," *Frontiers Neurorobot.*, vol. 13, p. 34, May 2019.

[51] Y.-L. Park et al., "Design and control of a bio-inspired soft wearable robotic device for ankle–foot rehabilitation," *Bioinspiration Biomimetics*, vol. 9, no. 1, Jan. 2014, Art. no. 016007.

[52] L. Roveda et al., "Model-based reinforcement learning variable impedance control for human–robot collaboration," *J. Intell. Robot. Syst.*, vol. 100, no. 2, pp. 417–433, Nov. 2020.